Solar Energy Materials and Solar Cells 187 (2018) 263–272

Contents lists available at ScienceDirect

Solar Energy Materials and Solar Cells

journal homepage: www.elsevier.com/locate/solmat

Determining the charge states and capture mechanisms of defects in silicon through accurate recombination analyses: A review

Fiacre E. Rougieux[a,*], Chang Sun[b], Daniel Macdonald[b]

[a] School of Photovoltaic and Renewable Energy Engineering, The University of New South Wales, Sydney NSW2052, Australia
[b] Research School of Engineering, College of Engineering and Computer Science, The Australian National University, Canberra ACT2601, Australia

ARTICLE INFO

Keywords:
Temperature and Injection Dependent Lifetime Spectroscopy
Deep Level Transient Spectroscopy
Recombination
Capture cross section
Defects
Silicon

ABSTRACT

A key strategy for further reducing the cost of solar electricity is through the development and production of very-high efficiency silicon solar cells (> 25%). The challenge in achieving this goal lies in overcoming limitations imposed by the electronic quality of the silicon wafers themselves. To overcome this challenge, it is necessary to understand the defects limiting the electronic quality of silicon wafers. In this review, we critically assess recent progress in understanding the recombination properties of defects in silicon and provide a nuanced and detailed picture of what constitutes accurate recombination parameters for such defects. Here we show that lifetime spectroscopy and capacitance spectroscopy analyses contain significant limitations, namely disregard of multivalent defect recombination in lifetime spectroscopy analyses, lack of exciton capture mechanisms in some deep level capacitance spectroscopy measurements and limitations in using detailed balance to extract capture parameters in capacitance spectroscopy. We demonstrate that combining multiple analyses leads to a more robust determination of recombination parameters. We use such combined analyses to review recombination pathways and parameters for technology relevant defects with the goal of enabling robust simulation of the lifetime in silicon for solar cell applications.

1. Introduction

The original Westinghouse study reported the normalized efficiency of silicon solar cells as a function of impurity concentration for a wide range of transition metals [1]. Since then, device architectures have dramatically improved and evidently the impact of impurities is felt at even lower concentrations, as shown by the recent studies of Riepe et al., Coletti et al., and Schmidt et al. [2–4]. The work of Graff and more recently Peaker et al. are excellent reviews of the energy levels and majority capture cross sections of metallic point defects in silicon [5,6]. For solar cell modelling and defect identification, accurate data on minority capture cross sections of defects are also required to allow modelling of their impacts on silicon solar cells, as well as a more nuanced approach to modelling the impact of defects, taking into account the limitations of the current literature. Three major sources of uncertainties currently exist as follows:

1) Temperature and Injection Dependent Lifetime Spectroscopy (TIDL [7] S) analyses are sometimes conducted using two or more independent energy levels (as is the case for Ti, Co and sometimes for Zn and Au) whereas they should be conducted using two or more dependent energy levels using the Sah and Shockley formalism [8].

2) Deep Level Transient Spectroscopy (DLTS) measurements are conducted with injection of only one type of carrier. As such, capture mechanisms operating via exciton enhanced Auger phenomena cannot take place, as exciton, are not present in significant concentrations when only one carrier is injected. This means the capture mechanism measured by DLTS may not be representative of the real capture mechanism in a device with both minority and majority carrier injection.

3) Determination of capture cross sections from DLTS emission data using detailed balance can yield capture cross sections with values orders magnitude higher or smaller than the actual capture cross section.

In this review, we apply the above three considerations to critically assess existing experimental data of defect recombination activity. We bring together a consistent set of values extracted from the literature for the modelling of point and extended defects in silicon. When necessary, the reported values are also corrected for different assumed values of the thermal velocities. We also review the temperature dependence of the majority and minority capture cross sections as well as more complex parameterizations of defect recombination such as via thermal donors, metal precipitates and dislocations.

* Corresponding author.
E-mail address: fiacre.rougieux@unsw.edu.au (F.E. Rougieux).

https://doi.org/10.1016/j.solmat.2018.07.029
Received 14 February 2018; Received in revised form 20 July 2018; Accepted 27 July 2018
Available online 23 August 2018

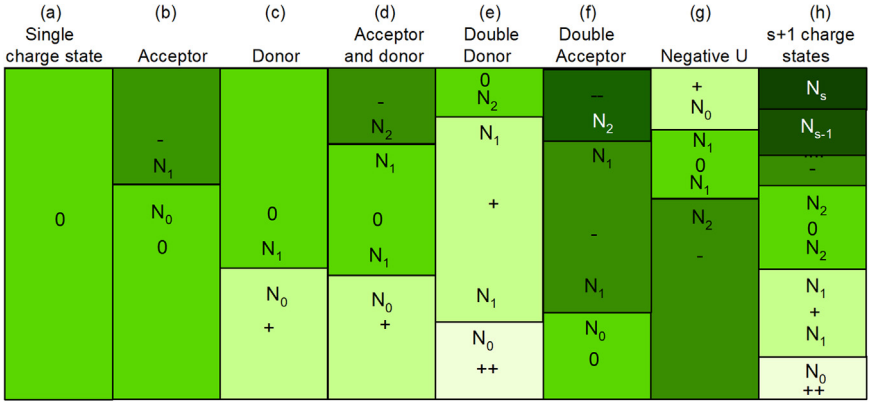

Fig. 1. Possible defect charge states and energy level associated with transitions between charge states.

2. Background

2.1. Charge states, energy levels and occupation fraction

A defect with a single charge state (Fig. 1a) does not allow recombination and trapping events since capture or emission of carriers are not allowed. This is the case of some light elements in silicon.

DLTS and Electron Paramagnetic Resonance (EPR) studies indicate that defects such as interstitial chromium, molybdenum, tungsten and iron can have two charge states (a single level within the bandgap). For a defect with two charge states (Fig. 1b and c) in non-equilibrium steady state both charge states remain at constant concentrations. On average, from a positive charge-state for a + /0 defect the following events can happen:

1) capture an electron and then capture a hole: $D^+ + e^- \rightarrow D^0$ followed by $D^0 + h^+ \rightarrow D^+$
2) capture an electron and then emit an electron: $D^+ + e^- \rightarrow D^0$ followed by $D^0 \rightarrow D^+ + e^-$
3) emit a hole and then capture a hole: $D^+ \rightarrow D^0 + h^+$ followed by $D^0 + h^+ \rightarrow D^+$

Thus, for a defect with two charge states, there is a single possible recombination event with:

1) capture an electron and then capture a hole: $D^+ + e^- \rightarrow D^0$ followed by $D^0 + h^+ \rightarrow D^+$

Modelling the impact of single level defects on the minority carrier lifetime can be simply performed using the full [9,10] or the simplified SRH formalism [11] provided that both capture mechanisms involve a single carrier (eg they are not defect-related Auger capture processes [12–16]).

Most defects are multivalent defects including titanium, vanadium, manganese, cobalt, nickel, palladium, platinum, cobalt, gold and zinc [6]. While often modelled with two or more independent levels in the IDLS and TIDLS literature, such defects should in principle be modelled with dependent levels according to the formalism derived by Sah and Shockley and others [8,17]. In contrast to assuming independent levels, the relative population of dependent levels depends on the position of the fermi level, and as such on the doping and injection level. Fig. 1 illustrates different types of defects with more than two charge states .

For a defect with three charge states (two levels, Fig. 1d, e, f and g) in non-equilibrium steady state, again all charge states remain at constant concentrations. On average, from a positive charge-state for a + + / + /0 defect we can:

1) capture an electron and then capture a hole: $D^+ + e^- \rightarrow D^0$ followed by $D^0 + h^+ \rightarrow D^+$
2) capture an electron and then emit an electron: $D^+ + e^- \rightarrow D^0$ followed by $D^0 \rightarrow D^+ + e^-$
3) emit a hole and then capture a hole: $D^+ \rightarrow D^0 + h^+$ followed by $D^0 + h^+ \rightarrow D^+$
4) capture a hole and then capture an electron: $D^+ + h^+ \rightarrow D^{++}$ followed by $D^{++} + e^- \rightarrow D^+$
5) capture a hole and then emit a hole: $D^+ + h^+ \rightarrow D^{++}$ followed by $D^{++} \rightarrow D^+ + h^+$
6) emit an electron and then capture an electron: $D^+ \rightarrow D^{++} + e^-$ followed by $D^{++} + e^- \rightarrow D^+$

Thus, for a defect with three charge states there are, two possible recombination events with:

1) capture an electron and then capture a hole: $D^+ + e^- \rightarrow D^0$ followed by $D^0 + h^+ \rightarrow D^+$
4) capture a hole and then capture an electron: $D^+ + h^+ \rightarrow D^{++}$ followed by $D^{++} + e^- \rightarrow D^+$

Essentially, a three charge states defect (or two-level defects) allows for two recombination pathways instead of one. As the injection level changes, the relative strength of these two recombination pathway changes reflecting the change in the different charge state density. Capacitance transient spectroscopy typically sees process 2, 3, 5 and 6 and thus can clearly identify multivalent defects provided the emission rate are different. Lifetime spectroscopy only sees recombination processes 1 and 4 lumped together and on its own cannot distinguish between multivalent and monovalent levels. However, a combination of both techniques allows such identification.

Note that the defect energy level represents the energy associated with a charge state transition, the intrinsic properties of individual defects being their charge states (the defect energy level is not the energy of a defect, in fact such quantity does not exist and does not make sense).

For a defect with s + 1 charge states (s levels, Fig. 1h) in non-equilibrium steady state, again all charge states remain at constant concentrations. The sum of the occupation of the charge states of the defect center is equal to:

$$N_0 + N_1 + ... + N_s = N_t \quad (1)$$

where the index represents the number of electrons on the defect center. The occupation ratio α for an energy level E(1/2) represents the occupation fraction of two consecutive charge states [18]:

$$\alpha_{1/2} = \frac{N_0}{N_1} = \frac{k_{1/2} n_{1/2} + p}{k_{1/2} n + p_{1/2}} \quad (2)$$

$$\alpha_{3/2} = \frac{N_1}{N_2} = \frac{k_{3/2} n_{3/2} + p}{k_{3/2} n + p_{3/2}} \quad (3)$$

More generally:

$$\alpha_{(2s-1)/2} = \frac{N_{s-1}}{N_s} = \frac{k_{(2s-1)/2} n_{(2s-1)/2} + p}{k_{(2s-1)/2} n + p_{(2s-1)/2}} \quad (4)$$

where $n_{(2s-1)/2}$ and $p_{(2s-1)/2}$ represent the ratio of the electron and hole

emission over electron and hole capture constants: $n_{(2s-1)/2} = e_{n(2s-1)/2}/c_{n(2s-1)/2}$, $p_{(2s-1)/2} = e_{p(2s-1)/2}/c_{p(2s-1)/2}$.

The occupation of the charge state s is Ns:

$$N_s = \frac{N_t}{1+\frac{1}{\alpha_{1/2}} + \frac{1}{\alpha_{1/2}\alpha_{3/2}} + ... + \frac{1}{\alpha_{1/2}\alpha_{3/2}...\alpha_{(2s-1)/2}}} \quad (5)$$

and subsequent levels using Eqs. (5)–(7).

The recombination rate associated with each recombination pathway can then be calculated using the generalized formula in the following section of this paper. Note that the occupation of each charge state must be recalculated for each injection level as the charge distribution will change.

The total lifetime is then the inverted sum of the inverted lifetimes:

$$\tau = \frac{1}{\frac{1}{\tau_0} + \frac{1}{\tau_1} + ... + \frac{1}{\tau_s}} \quad (6)$$

2.2. Capture mechanisms: dependence on carrier density and temperature

The temperature dependence of the capture cross section essentially depends on how the energy from the capture is dissipated. The energy can be dissipated through multi phonon emission, cascade, radiative emission and defect reactions [19–21]. In addition, the energy can be dissipated through secondary carrier excitation via an Auger process [12–14,22]. During Multiphonon Emission capture (MPE), the energy and momentum of the electronic state is transferred simultaneously to phonons. For cascade capture, the energy and momentum of the electronic state is transferred by emission of a series of phonons, with the electron cascading down the levels. For the Auger Capture (AC) and Excitonic Auger Capture mechanism (EAC), the energy and momentum of the electronic states is transferred to a third carrier. Finally, during radiative recombination, photons are emitted with accompanying phonons to allow for momentum conservation.

For a full electron-hole pair annihilation there must be both capture of an electron and a hole. Recombination will take place after a combination of two of the above capture phenomena have taken place [23]. For instance, an electron could be captured by exciton-enhanced Auger-recombination whilst a hole is captured by a multiphonon-emission capture, leading to a full electron-hole recombination event.

In silicon, our review shows that Exciton-enhanced Auger and phonon emission processes dominate capture mechanisms. Both processes are described below and shown in Fig. 2. More detailed descriptions of other processes are included in the Appendix.

The multiphonon process requires sufficient phonons to enable the energy level of the defect to cross an occupied conduction band state. The equilibrium distribution of phonons is given by the Bose-Einstein distribution as $f(E) = 1/(\exp(E/k_BT)-1) \approx \exp(-E/k_BT)$. As the concentration of energetic phonons increases, the capture-cross section increases [19]. The capture cross section is then proportional to $\exp(-E/k_BT)$ and increases with temperature [19]. The greater the strength of the electron-phonon coupling the greater the capture cross section of defects operating with this capture mechanism. The transition rate for electron trapping and hole trapping corresponding to the two multiphonon capture processes are [24]:

$$U_n = \sigma_n v_{th}(np_t - n_1 n_t) \quad (7)$$

$$U_p = \sigma_p v_{th}(pn_t - p_1 p_t) \quad (8)$$

With n_t and p_t the electron and hole concentration in the level. Considering $N = n_t + p_t$, the net recombination rate corresponding to capture of a hole and an electron through multiphonon capture mechanism becomes the standard SRH recombination rate [24]:

$$U = \frac{np - n_i^2}{\tau_{p0}(n + n_1) + \tau_{n0}(p + p_1)} \quad (9)$$

with $\tau_{p0} = 1/N_t\sigma_p v_{th}$ and $\tau_{n0} = 1/N_t\sigma_n v_{th}$.

Excitonic Auger Capture processes relies on the existence of excitons for the recombination to take place [12,13,25]. Essentially, when an exciton approaches an impurity, the electron (or hole) is captured by the impurity and the hole (or electron) is excited into the band. Following this another exciton approaches the impurity and a hole (or electron) is captured by the impurity and the electron (or hole) is excited into the conduction band. This concludes the full recombination of an electron-hole pair using two excitons [13]. The exciton density is determined by the density of free carriers n and p, the temperature, the effective masses, the exciton binding energy E_{ex} and degeneracy g_{ex} as [26,27]:

$$n_{ex} = \frac{np}{\frac{\sqrt{N_c N_V}}{f} exp\left(\frac{-E_{ex}}{k_B T}\right)} \quad (10)$$

$$f = \sqrt{g_{ex}}\left[\frac{1+m_e/m_h}{\sqrt{m_e/m_h}}\right]^{3/2} \quad (11)$$

At 25 °C, for a doping density of $N_D = 1.0 \times 10^{15}$ cm^{-3} and an injection level of $\Delta n = 1.0 \times 10^{15}$ cm^{-3}, the exciton density is 1.2×10^{11} cm^{-3}. Taking an exciton binding energy of $E_{ex} = 14.7$ meV, the exponential remains close to unity (less than 10 at temperatures above 100 K) and the main temperature dependence of the exciton concentration arises from the power law dependence of the conduction and valance band effective density of states [28,29]:

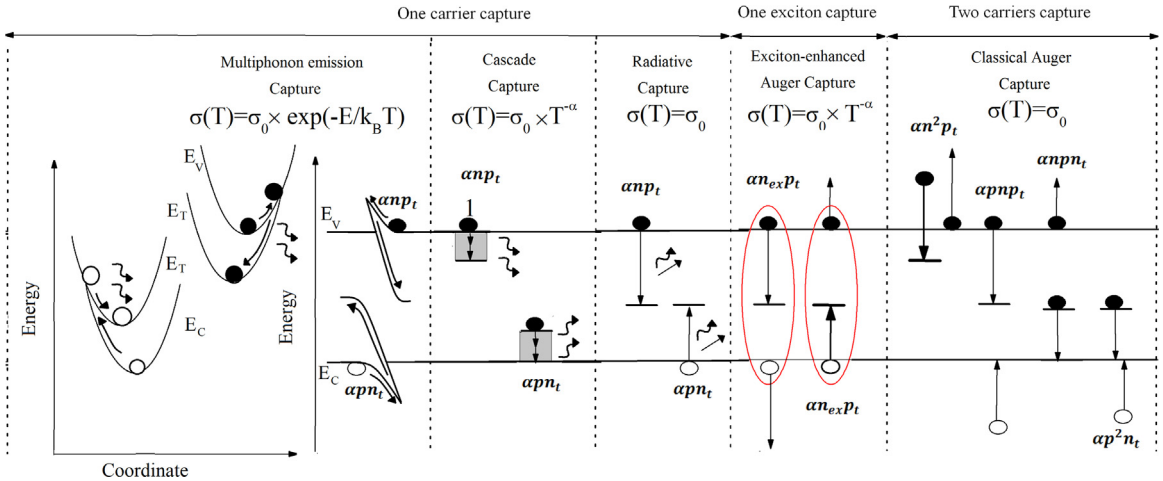

Fig. 2. Schematic representation of five possible capture mechanisms. Our review shows that multiphon emission capture and exciton-enhanced Auger capture are the main capture mechanisms in silicon.

$$N_C = 2\left(\frac{2\pi m^*_{dc} k_B T}{h^2}\right)^{3/2} \quad (12)$$

$$N_V = 2\left(\frac{2\pi m^*_{dv} k_B T}{h^2}\right)^{3/2} \quad (13)$$

The capture cross section has then a power law $T^{-\alpha}$ dependence on temperature and decreases with temperature [13]. The exciton Auger capture process also differs from the classical Auger process in the involvement of excitons. As such, the recombination rate depends linearly on the exciton density rather than quadratically on the carrier density.

One important question remains though, can we use Eq. (9) (the standard SRH recombination rate) to calculate the net recombination rate related to capture trough exciton-enhanced defect Auger processes? The net SRH recombination rate is derived from the continuity equations for electron and holes and some authors have in addition used a continuity equation for excitons to describe exciton-enhanced recombination [14,15]. The time constants for exciton pairing and dissociation are in the picoseconds and thus for the minority carrier lifetime in silicon (usually above 1 μs), the exciton population and free carrier populations are effectively in equilibrium steady-state relative to each other. Thus, Eq. (9) can be successfully used to calculate exciton-enhanced defect Auger capture although it is intrinsically an exciton mechanism. This is not the case for free carrier defect Auger capture, where quadratic terms need to be inserted in the SRH equation, see Appendix for further details.

3. Limitation in lifetime spectroscopy analyses and capacitance transient spectroscopy analyses

3.1. Lifetime spectroscopy and dependent energy levels

An inaccuracy arising from some TIDLS analyses is that defects are modelled as independent levels, whilst from Transient Capacitance studies the levels are known to be dependent. Modelling dependent levels as independent can yield erroneous energy levels and capture cross-sections. Another common practice is to model multivalent defects with only one defect. This is often justified in that one level "dominates" the recombination activity and thus the other can be ignored. A level only dominates for a limited range of dopant density and injection levels. Although the parametrization may fit the data for the injection levels and single dopant concentration used in the study, it will not be generalizable to all injection levels and dopant density. A better way to make sure all levels are detected is to make sure that a wide injection range is chosen and by varying the doping by orders of magnitude and doing measurements both in p-type and n-type silicon. This will ensure the Fermi level and quasi Fermi levels sweep all possible energetic combinations within the bandgap and thus a combination of all charge states of the defect are present in all measurements.

Simple modelling using the above expressions shows that this is often not the case. As such TIDLS analysis using single level or independent levels, when there are multiple dependent levels present, may lead to grossly inaccurate defect parameters.

3.2. DLTS and exciton-enhanced Auger recombination

One drawback of capacitance spectroscopy is that field effects may play a role in changing the capture and emission parameters of defects for instance due to trap assisted tunnelling effects, impact ionization and Pool-Frenkel effects [30–32].

A further complication with DLTS on Schottky diodes is that it measures the capture-cross section under majority carrier injection only. As such the concentration of excitons is small and Excitonic Auger capture does not take place. For the purpose of modelling silicon under both majority and minority carrier injection (eg solar cell operation), one needs to take into account possible Excitonic Auger capture processes. Measurements where the sample is excited optically with energy above bandgap (TIDLS or MCTS) or forward bias pn junction have an advantage here. If the capture cross sections as measured by optical excited measurements can be shown to be larger than those measured by DLTS, and they have a power law temperature dependence, then Excitonic Auger capture may be more efficient than the capture measured by DLTS. In such cases the parameters determined by optically excited methods should be used to model the defect. Note that Optical DLTS (where below bandgap excitation is used to optically excite a defect) is not useful here as it does not generate free excitons.

3.3. Note on energy level, Gibbs free energy, enthalpy and entropy

The energy for charge transition of a defect is the Gibbs Free Energy:

$$\Delta G = E_C - E_T \quad (14)$$

When the injection level or temperature changes there is a change in the defect charge state which leads to a change of entropy related to the configuration and lattice vibrations as bound electrons and holes at the center influence its coupling to the lattice. The energy for charge state transition contains an enthalpy term and an entropy term:

$$E_C - E_T = \Delta H - T\Delta S \quad (15)$$

For instance, combined optical and electrical measurements of tungsten contaminated samples has shown that the energy for charge state transition of tungsten in silicon has an enthalpy term of 0.383 eV and an entropy term of 8.2×10^{-5} eV K^{-1} [33].

Lifetime spectroscopy measurements involve a range of injection and thus a range of charge state density (for instance see [34]). TIDLS measurements involve both a range of injection levels and temperature, leading to a wide range of defect occupancy. Thus, the energy measured by lifetime spectroscopy and TIDLS is the enthalpy for charge state change not the energy for charge state change.

$$n_1 = gN_C exp\left(\frac{E_C - E_T}{k_B T}\right) \quad (16)$$

$$n_1 = gN_C exp\left(\frac{\Delta S}{k_B}\right) exp\left(\frac{-\Delta H}{k_B T}\right) \quad (17)$$

The same holds true for transient spectroscopy measurements and is well summarized in [35].

The emission rate from a defect is [36]:

$$e_n = g\sigma_n v_{th} N_C exp\left(\frac{E_C - E_T}{k_B T}\right) \quad (18)$$

where g is the change in degeneracy upon emission, with Eq. (11) this becomes:

$$e_n = g\sigma_n v_{th} N_C exp\left(-\frac{\Delta H - T\Delta S}{k_B T}\right) \quad (19)$$

Which becomes:

$$e_n = g\sigma_n v_{th} N_C exp\left(\frac{\Delta S}{k_B}\right) exp\left(\frac{-\Delta H}{k_B T}\right) \quad (20)$$

A common DLTS analysis technique to determine activation energies and capture cross sections is through an Arrhenius plot. This technique relies on detailed balance to obtain the capture cross section and energy level by measuring the emission rate at different temperatures [35]:

$$ln(e_n) = ln(g\sigma_n v_{th} N_C) + \frac{\Delta S}{k_B} - \frac{\Delta H}{k_B T} \quad (21)$$

The slope and origin $\ln(e_n)$ is often assumed to yield the energy level and capture cross section respectively. Instead the slope and origin of $\ln(e_n)$ yield the enthalpy of the charge state transition and the capture cross section containing an entropy term. Thus, such quantities must be corrected [35].

Such considerations are particularly important when comparing energy levels determined electrically (Enthalpy) and optically (Gibbs free energy) for instance comparing conventional DLTS or lifetime spectroscopy measurements to photoluminescence measurements or optical DLTS measurements. Whilst the enthalpy level determined by transient spectroscopy and lifetime spectroscopy may be very similar (the enthalpy is almost temperature independent [35]), the actual energy level in both measurements may be significantly different due to the different occupation fraction in the two measurements.

3.4. DLTS, Arrhenius plots and detailed balance

A further complication arise with detailed balance in that this analysis often assumes a temperature independent majority capture cross section, which is almost never the case in practice as shown in below. (the topic of inaccuracies in energy levels obtained from Arrhenius plots is discussed in [35,37]). One way this is often accounted for is by assuming that the capture cross section is thermally activated [36]:

$$\sigma_n = \sigma_{n_\infty} exp\left(\frac{-E_\infty}{k_B T}\right) \tag{22}$$

The slope and origin of the $\ln(e_n)/T^2$ 1/T graph, thus yield the energy level and capture cross section, provided that energy level is corrected by the activation energy for carrier capture as follows:

$$ln(e_n) = ln\left(g\sigma_{n_\infty} v_{th} N_C\right) - \frac{E_T + E_\infty}{k_B T} \tag{23}$$

This approach assumes that capture is thermally activated in the form of an exponential. However as seen in Section 3, the temperature dependence can have a more complex form, including power laws and combined power and exponential dependences. Thus, the most accurate way to determine the capture cross section and energy level is by direct measurements of these quantities, for example by the pulse-width variable m4

4. Point defects: review

4.1. Data selection methodology

The data was selected based on the following criteria:

1) Multivalent level: Lifetime spectroscopy and TIDLS only selected if performed with multivalent level analyses unless the defect is known to have only two charge states from Transient Capacitance.
2) Temperature dependent Capture: Transient Capacitance Spectroscopy is selected only if performed using pulse filling method.
3) Exciton-enhanced Auger process: There is agreement between DLTS measurements and measurements where the sample is excited optically (TIDLS or MCTS) or DLTS with forward bias of a pn junction.

Throughout the text, the quoted defect energy level is the enthalpy not the Gibbs free energy.

4.2. Process for identification of capture mechanism

To identify the capture mechanisms, we used the dependence of the capture cross section on the temperature and the dependence of the recombination rate on the free carrier concentration and followed this process:

1) Capture mechanisms having a thermally activated behaviour are assumed to consist of multiphonon emission [19].
2) Capture mechanisms having a power law temperature dependence are assumed to consist either of exciton-enhanced Auger capture or cascade capture [12,13].
   a. When direct evidence of Auger capture is present (through measurements of luminescence near almost twice the bandgap of highly excited Auger carriers), the mechanism is set to exciton-enhanced Auger capture [12,13].
   b. If capture is into non-coulombicnon-coulombic repulsive center (the charge state of the defect is neutral or of similar polarity to the free carrier to be captured), the mechanism is set to exciton-enhanced Auger Capture [12,13].
   c. If capture is into a deep attractive center, the mechanism is set to exciton-enhanced Auger Capture [12,13].
   d. If capture is into a shallow attractive center, the mechanism is set to cascade capture [12,13].
3) Capture mechanisms involving no temperature dependence are assumed to consist either of multiphonon-emission capture with an activation energy close to 0 or to defect Auger capture involving free carriers [19,24]
   a. If the recombination rate is shown to depend quadratically on the carrier density, the mechanism is set to defect Auger recombination involving free carriers [24].
   b. Otherwise the capture mechanism is set to multiphonon emission with low activation energy [19].

4.3. Energy level and capture cross section at room temperature

Fig. 3 summarizes the energy level and charge state of defects in silicon. Most energy levels are extracted from DLTS measurements or TIDLS measurements. It is clear from this Fig. that most defects are multivalent defects in silicon and as such their parameters must be modelled using the Sah and Shockley formalism [8].

The energy levels and capture cross sections of common defects are listed in Table 1 of Appendix A. The energy levels are quoted relative to the bottom of the conduction band. The subscript i indicates an interstitial impurity and the subscript s indicates a substitutional impurity.

There remain significant contradictions in the literature regarding the number of charge states that certain defects can take. DLTS assumes that a different emission peaks constitutes the different levels of the same defect if after annealing, the concentration of all levels change similarly. However, this assumption can sometimes fail, for example with the formation of transition metal-acceptor pairs or with the formation of recombination-active transition-metal hydrogen pairs. This is where lifetime spectroscopy is complimentary as by sweeping a range of injection levels, it allows to sweep a range of relevant charge states and allows to validate transient spectroscopy data.

4.4. Capture mechanisms and temperature dependence

The parametrization of the temperature dependence of the capture cross sections is listed in Table 1 of Appendix B for known impurities, together with suggested physical mechanisms responsible for carrier capture. For some impurities, the majority carrier capture cross section is extracted from the DLTS measurements using an extrapolation of temperature dependent cross-section measurements to 300 K. For others, the minority carrier capture cross section is reported from Injection Dependent Lifetime Spectroscopy (IDLS) measurements or from TIDLS measurements. Fig. 4 summarizes the results in Table 1 and shows the most likely capture mechanisms at common defects in silicon according to our review. Most capture cross sections in silicon are temperature dependent. It is apparent that recombination consisting of different capture mechanisms for electrons and holes are very common in silicon. This underlines the importance of taking into account the temperature dependence of capture cross sections when analysing DLTS or TIDLS measurements.

Significant uncertainties remain in assigning capture mechanisms in silicon. For instance, distinguishing between exciton-enhanced Auger capture and Cascade capture remains challenging. Techniques able to measure the energy of hot carriers generated by defect Auger process

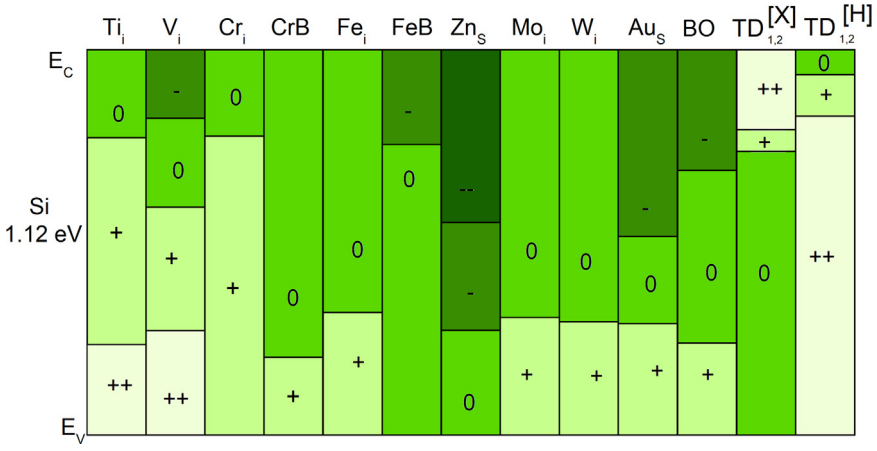

Fig. 3. Energy levels and charge state of dominant defects in silicon.

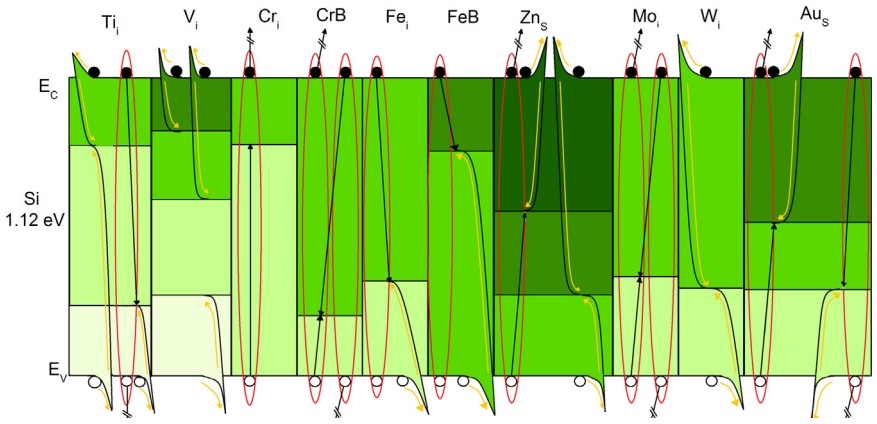

Fig. 4. Suggested capture mechanisms leading to recombination at common defects.

can greatly increase our confidence in the nature of capture mechanisms. Luminescence spectroscopy has been shown to be a powerful tool to directly observe exciton-enhanced defect Auger-related hot-electrons [12,13].

Distinguishing between cascade capture and two stage cascade capture is also potentially difficult as the multiphonon part of the second stage can have a very low activation energy and thus both phenomenon can have very similar temperature dependence.

5. Modelling recombination at extended defects in silicon

Some defects cannot be modelled using multivalent recombination statistics. This is the case of Metallic precipitates and dislocations as these form Schottky contacts and thus lead to a different form of recombination. Modelling of such defects is briefly summarized below.

5.1. Metallic precipitates

Typical impurities existing in the form of precipitates in silicon include Cobalt, Nickel, Copper, Zinc and Palladium. Metallic precipitates behave differently to single metallic atoms. Precipitates can form internal Schottky contacts surrounded by a space charge region which can be an order of magnitude greater than their geometrical size. The radius of this space charge region depends on the precipitate itself, the doping density and the excess carrier density. Thermionic emission is the dominant mechanism for recombination at such precipitates and therefore a full numerical simulation (solving Poisson equations and the continuity equations simultaneously) must be used to simulate the impact of precipitates on the lifetime. An alternative is to use a parametrization of the recombination based on existing numerical simulations. A full parametrization has been suggested by Kwapil et al. who used a max min approach to parametrize the capture cross section of metallic precipitates as a function of excess carrier density and doping [38,39]:

$$\sigma_{prec} = r_{prec}^2 \times \left[\sigma_{min} + \frac{\sigma_{max} - \sigma_{min}}{1+(\Delta n/\Delta n_{ref})^{alpha}} \right] \quad (24)$$

where r_{prec} is the actual precipitate radius. For the full parametrization see Refs. [38,39].

5.2. Dislocations

Recombination at dislocations is highly complex as it depends on the charge accumulated at the dislocations as well as the level of metallic decoration [40–42]. Practically and more simplistically, dislocations can be approximated by a cylinder penetrating the depth of the silicon wafer. This recombination cylinder is characterized by a recombination strength γ_d, which is a free parameter. A typical value for γ_d is 4×10^{-2} cm^2 s^{-1}. In the model of Kieliba et al. based on the models of Donolato and Kweder, the recombination strength is used to calculate an effective diffusion length [43–45]:

$$\frac{1}{L_{eff}} = \frac{1}{L_0} + \frac{2}{\pi}\rho_d \Gamma_d \int_0^{\infty} \frac{k^2}{\mu^2} \frac{dk}{1+(\Gamma_d/\pi)H(\mu\varepsilon, \mu a)} \quad (25)$$

with L_0 the diffusion length in the material without dislocations, ρ_d the dislocation density, $\Gamma_d = \gamma_d/D$ the normalized recombination strength, $\mu = (k^2 + 1/L_0^2)^{0.5}$ and [43]:

$$H(\mu\varepsilon, \mu a) = \frac{1-\mu\varepsilon K_1(\mu\varepsilon)}{\mu^2\varepsilon^2} + \frac{I_1(\mu\varepsilon)K_1(\mu a)}{\mu\varepsilon I_1(\mu a)} \quad (26)$$

with I_1 and K_1 the modified Bessel functions of order one I_1 and K_1

The injection dependent effective diffusion length can then be used to calculate the injection dependent carrier lifetime using an injection dependent mobility model [43,44].

6. Conclusions

There are significant inconsistencies in the recombination parameters of point defects in the literature. In this paper, we highlight three fundamental sources of inconsistencies. Within lifetime spectroscopy analyses, modelling multivalent defect as monovalent defect leads to parameters that are not generalizable to all dopant density and injection levels. Using detailed balance also leads to inaccurate defect parameters in capacitance spectroscopy analyses. Finally, exciton enhanced auger recombination, one of the most frequent defect capture mechanism, can only be measured using both minority and majority carrier injection and thus using lifetime spectroscopy or capacitance spectroscopy with above bandgap optical excitation. Lifetime spectroscopy and capacitance transient spectroscopy are two complimentary techniques and most often both are needed to fully characterize the recombination properties of defects and identify their charge states and recombination mechanisms.

By leveraging these three principles, we provide a consistent set of recombination parameters for modelling the lifetime limited by point and extended defects in silicon wafers and devices. We summarize the main capture mechanisms driving recombination in silicon. Finally, we briefly review examples of recombination at extended defects. This set of parameters is well suited to understand and model the impact of point defects on the lifetime in a wide range of temperatures, and the influence of extended defects at room temperature. More generally, the limitations of current defect recombination analyses outline in this paper, enable more robust defect analyses, identification and modelling in silicon solar cells.

Complimentary techniques such as luminescence spectroscopy (photo and electro) will be valuable tools to cross-validate some of the capture mechanisms suggested in this paper (reviewed from transient spectroscopy and lifetime spectroscopy measurements). Combined lifetime spectroscopy and capacitance spectroscopy on the same samples are likely to enable more robust determination of defect energy levels and charge states.

Acknowledgements

This work was supported by the Australian Research Council (ARC) Discovery Early Career Researcher Award (DECRA) project DE160101368.

Appendix A

In the cascade capture model, the energy dissipation sees the electron cascading down excited energy levels of the defect [20]. There is no change of charge state associated with these levels, such levels are simply the excited states of the electron from the ground state of the impurity in the hydrogenic model. The electron loses energy by electron phonon interactions falling down to the ground state. This process requires the existence of many excited states of the defect and requires the electrons to not be reemitted at one of the intermediate energy levels. As the temperature increases, the probability that the electron will be reemitted increases. As such, the capture cross section decreases with temperature. Most often the last transition involves a significant amount of energy release, which cannot be achieved through phonon. Thus, Cascade capture is often combined with a multiphonon emission process into the ground state of the defect leading to a combined power law and exponential temperature dependence if the activation energy for the multiphon process is high [46]. If the activation energy for the multiphon process is low it simply leads to a power law dependence on temperature. Being a one carrier capture process the transition rate for electron trapping and hole trapping is essentially the same as the multiphonon emission process and the radiative process:

$$U_n = \sigma_n v_{th}(np_t - n_1 n_t) \quad (27)$$

$$U_p = \sigma_p v_{th}(pn_t - p_1 p_t) \quad (28)$$

Cascade capture arises, in principle from shallow levels and thus capture of the carrier with opposite polarity will occur with a different mechanism. If capture of the other carrier is a one carrier capture mechanism, the net recombination rate will be:

$$U = \frac{np - n_i^2}{\tau_{p0}(n + n_1) + \tau_{n0}(p + p_1)} \quad (29)$$

with $\tau_{p0} = 1/N_t\sigma_p v_{th}$ and $\tau_{n0} = 1/N_t\sigma_n v_{th}$.

Auger capture mechanisms in particular exciton enhanced trap assisted Auger capture mechanisms occur in silicon [12,13,24]. It is less clear, if defect-Auger capture mechanism involving free carriers is a significant mechanism in solar cell operation (in laser and other high-injection range it is more likely to be dominant). Defect-assisted Auger capture mechanisms involve three particles, an electron and a hole recombine and the energy and momentum is transferred to a third particle. The capture probability has a weak temperature dependence as it mainly depends on the carrier concentration. On the other hand, the recombination rate depends quadratically on the carrier density. The transition rates for electron trapping and hole trapping corresponding to the four defect Auger capture processes are [24]:

$$U_{nn} = \sigma_{nn} v_{th} n(np_t - n_1 n_t) \quad (30)$$

$$U_{np} = \sigma_{np} v_{th} p(np_t - n_1 n_t) \quad (31)$$

$$U_{pn} = \sigma_{pn} v_{th} p(pn_t - p_1 p_t) \quad (32)$$

$$U_{pp} = \sigma_{pp} v_{th} n(pn_t - p_1 p_t) \quad (33)$$

The net recombination rate corresponding to capture of a hole and an electron through defect-assisted Auger capture mechanisms is different than the standard SRH recombination rate in that the perfectors to the electron and hole concentrations are now injection dependent [24]:

$$U = \frac{np - n_i^2}{\tau_{p0}^*(n + n_1) + \tau_{n0}^*(p + p_1)} \quad (34)$$

with $\tau_{p0}^* = 1/N_t v_{th}(\sigma_{pp}p + \sigma_{pn}n)$ and $\tau_{n0}^* = 1/N_t v_{th}(\sigma_{nn}n + \sigma_{np}p)$

Appendix B

An alternative way to model the impact of the boron oxygen defect is to use the empirical parametrization of Bothe and Schmidt [66]. This parametrization of the lifetime is made at an injection level of injection $\Delta n = 0.1\ N_{doping}$ and is close to a parametrization of the minority carrier lifetime [66]:

$$\tau_n = 7.675 \times 10^{45} [B_S]^{-0.824} [O_i]^{-1.748} \quad (35)$$

Note that there are uncertainties associated with this parametrization as the concentration of BO defects depends on thermal history of the sample. Together with the knowledge of the energy levels and the capture cross-section ratios of the BO defect (as shown in Table 1), one can obtain the majority carrier lifetime and thus the injection dependent lifetime curve.

Table 1
Temperature dependence of the capture cross sections for different impurities. The suggested physical mechanism responsible for carrier capture is shown together with the expression and constants needed to model the temperature dependence of the capture cross sections. When lifetime spectroscopy is used, a transient spectroscopy measurement is also cited to validate the fact that a single level exist.

s + d	Impurity	Quantity	Suggested physical mechanism	Expression	σ_∞, σ_0	α	E_∞	Ref
4	Ti_i							
	$E_C - E_T$	σ_n	Multiphonon emission capture	$\sigma_\infty \times \exp(-E_\infty/k_BT)$	2.57×10^{-14}		***0.0039***	[47]
	0.27 eV	σ_p	Multiphonon emission capture	σ_0	1.35×10^{-15}			[47]
	$E_C - E_T$	σ_n	Excitonic Auger capture	$\sigma_0 \times T^{-\alpha}$	3.9×10^{-12}	1		[47]
	0.87 eV	σ_p	Multiphonon emission capture	$\sigma_\infty \times \exp(-E_\infty/k_BT)$	1.09×10^{-16}		***0.027***	[47]
5	V_i							
	$E_C - E_T$	σ_n	Multiphonon emission capture	σ_0	1.2×10^{-16}			[48]
	0.20 eV	σ_p						
	$E_C - E_T$	σ_n	Multiphonon emission capture	σ_0	5.3×10^{-15}			[48]
	0.45 eV	σ_p						
	$E_C - E_T$	σ_n						
	0.78 eV	σ_p	Multiphonon emission capture	$\sigma_\infty \times \exp(-E_\infty/k_BT)$	1.16×10^{-16}		***0.12***	[48]
6	Cr_i							
	$E_C - E_T$	σ_n						[49,50]
	0.24 eV	σ_p	Excitonic Auger capture	$\sigma_0 \times T^{-\alpha}$	2.8×10^{-12}	1.1		[49,50][b]
	CrB							
	$E_C - E_T$	σ_n	Excitonic Auger capture	$\sigma_0 \times T^{-\alpha}$	2.0×10^{-12}	1.2		[49,50][b]
	0.93 eV	σ_p	Excitonic Auger capture	$\sigma_0 \times T^{-\alpha}$	4.3×10^{-12}	1.2		[49,50 7][b]
8	Fe_i							
	$E_C - E_T$	σ_n	Excitonic Auger capture	$\sigma_0 \times T^{-\alpha}$	3.47×10^{-11}	1.48		[51,52]
	0.79 eV	σ_p	Multiphonon emission capture	$\sigma_\infty \times \exp(-E_\infty/k_BT)$	4.54×10^{-16}		***0.05***	[51,52]
	FeB							
	$E_C - E_T$	σ_n	Excitonic Auger capture	$\sigma_0 \times T^{-\alpha}$	5.1×10^{-19}	2.5		[51,52]
	0.26 eV	σ_p	Multiphonon emission capture	$\sigma_\infty \times \exp(-E_\infty/k_BT)$	3.32×10^{-10}		***0.262***	[51,52]
12	Zn_S							
	$E_C - E_T$	σ_n	Multiphonon emission capture	σ_0	9.9×10^{-16}			[53][a]
	0.84 eV	σ_p	Multiphonon emission capture	σ_0	2.0×10^{-14}			[53][a]
	$E_C - E_T$	σ_n	Multiphonon emission capture	$\sigma_\infty \times \exp(-E_\infty/k_BT)$	1.81×10^{-17}		***0.136***	[53][a]
	0.51 eV	σ_p	Excitonic Auger capture	$\sigma_0 \times T^{-\alpha}$	1.8×10^{-5}	3.93		[53][a]
6	Mo_i							
	$E_C - E_T$	σ_n	Excitonic Auger capture	$\sigma_0 \times T^{-\alpha}$	4.2×10^{-8}	1.07		[54,55]
	0.8 eV	σ_p	Excitonic Auger capture	$\sigma_0 \times T^{-\alpha}$	6.05×10^{-14}	2.95		[54,55]
6	W_i							
	$E_C - E_T$	σ_n	Multiphonon emission capture	$\sigma_\infty \times \exp(-E_\infty/k_BT)$	1.2×10^{-15}		***0.017***	[33,56][a]
	0.81 eV	σ_p	Multiphonon emission capture	$\sigma_\infty \times \exp(-E_\infty/k_BT)$	1.2×10^{-16}		***0.018***	[33,56][a]
11	Au_s							
	$E_C - E_T$	σ_n	Excitonic Auger capture	$\sigma_0 \times T^{-\alpha}$	2.9×10^{-11}	2.0		[57]
	0.82 eV	σ_p	Multiphonon emission capture	σ_0	3.5×10^{-15}			[57]
	$E_C - E_T$	σ_n	Multiphonon emission capture	σ_0	8.5×10^{-17}			[57]
	0.55 eV	σ_p	Excitonic Auger capture	$\sigma_0 \times T^{-\alpha}$	1.5×10^{-11}	1.3		[57]
Technology relevant defects								
	Ox prec[c]							
	$E_C - E_T$	σ_n	–	1.1×10^{-13}				[17,58]
	0.95 eV	σ_p	–	6.6×10^{-16}				[17,58]
	$E_C - E_T$	σ_n	–	1.1×10^{-14}				[17]
	0.08 eV	σ_p	–	1.3×10^{-11}				[17]
	BO[d]							
	$E_C - E_T$	σ_n / σ_p		18				[59–62]
	0.34 eV							
	$E_C - E_T$	σ_n / σ_p		1/60				[59–62]
	0.88 eV							
	Lvl1/Lvl2	$\sigma_{n1} / \sigma_{p2}$		0.2				[59–62]
	TD[e])							[63,64]
	$E_C - E_T$	σ_n		$3.16 \times 10^{-54} \times [X]^{2.41}$				[63,64]
	$15.46 \times [TD]^{-0.12}$	σ_p		$4.01 \times 10^{-40} \times [X]^{1.53}$				[63,64]

[a] Temperature dependent data reanalysed in this paper.
[b] σ_0 is fitted to obtain the literature value of σ at 300 K and using the exponent of Refs. [25] or [50].
[c] Note that for oxygen precipitates the capture cross section is the effective capture cross section of the whole precipitates assuming each precipitate has eight corners [17].
[d] The absolute concentration of the boron-oxygen defect is not known as the absolute values of the capture cross sections are not known (preliminary DLTS measurements show majority capture cross sections in the order of 1×10^{-18} and minority capture cross sections in the order of 1×10^{-17}, which would mean the defect should be highly concentrated to lead to the very low lifetime observed in p-type silicon) [65].

[e)]Thermal donors are a family of defects consisting of chains of oxygen atoms. The different members of the family are often labelled TD1, TD2…. TDn. The first two thermal donors, TD1 and TD2 exist in two structural configurations for a single charge state often labelled H and X [63]. *Tomassini et al.* showed that while the resistivity scales with the H configuration, the recombination activity (energy level and capture cross sections) depends on the concentration of the X configuration [64]:

$$[X] = 0.1268 \times [TD] + 3.956 \times 10^{13} \quad (36)$$

References

[1] J. Davis, A. Rohatgi, R.H. Hopkins, P.D. Blais, P. Rai-Choudhury, J.R. McCormick, H.C. Mollenkopf, Impurities in silicon solar cells, IEEE Trans. Electron Devices 27 (1980) 677–687, https://doi.org/10.1109/T-ED.1980.19922.

[2] S. Riepe, I.E. Reis, W. Kwapil, M. Falkenberg, J. Schön, H. Behnken, J. Bauer, D. Kreßner-Kiel, W. Seifert, W. Koch, Research on efficiency limiting defects and defect engineering in silicon solar cells - results of the German research cluster SolarFocus, Phys. Status Solidi (C) 8 (2011) 733–738, https://doi.org/10.1002/pssc.201000338.

[3] G. Coletti, Sensitivity of state-of-the-art and high efficiency crystalline silicon solar cells to metal impurities, Progress. Photovolt.: Res. Appl. 21 (2013) 1163–1170, https://doi.org/10.1002/pip.2195.

[4] J. Schmidt, B. Lim, D. Walter, K. Bothe, S. Gatz, T. Dullweber, P. Altermatt, Impurity-related limitations of next-generation industrial silicon solar cells, IEEE J. Photovolt. 3 (2012) 114–118, https://doi.org/10.1109/JPHOTOV.2012.2210030.

[5] A. Peaker, V. Markevich, B. Hamilton, G. Parada, A. Dudas, A. Pap, E. Don, B. Lim, J. Schmidt, L. Yu, Y. Yoon, G. Rozgonyi, Recombination via point defects and their complexes in solar silicon, Phys. Status Solidi (A) 209 (2012) 1884–1893, https://doi.org/10.1002/pssa.201200216.

[6] K. Graff, K. Graff, Metal Impurities in Silicon-Device Fabrication, 24 Springer, 1995, pp. 19–64, https://doi.org/10.1007/978-3-642-97593-6_3.

[7] S. Rein, Lifetime Spectroscopy, 85 Springer, 2005, pp. 69–255, https://doi.org/10.1007/3-540-27922-94.

[8] C.-T. Sah, W. Shockley, Electron-hole recombination statistics in semiconductors through flaws with many charge conditions, Phys. Rev. 109 (1958) 1103–1115.

[9] W. Shockley, W. Read, Statistics of the recombinations of holes and electrons, Phys. Rev. 87 (1952) 835–842, https://doi.org/10.1103/PhysRev.87.835.

[10] Hall, Electron-hole recombination in Germanium, Phys. Rev. 87 (1952), https://doi.org/10.1103/PhysRev.87.387 (387–387).

[11] D. Macdonald, A. Cuevas, Validity of simplified Shockley-Read-Hall statistics for modeling carrier lifetimes in crystalline silicon, Phys. Rev. B. 67 (2003), https://doi.org/10.1103/PhysRevB.67.075203.

[12] A. Hangleiter, Experimental proof of impurity Auger recombination in silicon, Phys. Rev. Lett. 55 (1985) 2976–2978, https://doi.org/10.1103/PhysRevLett.55.2976.

[13] A. Hangleiter, Nonradiative recombination via deep impurity levels in semiconductors: the excitonic Auger mechanism, Phys. Rev. B 37 (1988) 2594–2604, https://doi.org/10.1103/PhysRevB.37.2594.

[14] J. Blakemore, Semiconductor Statistics, (2002).

[15] Sachenko, Y. Kryuchenko, Recombination statistics and kinetics in semiconductor nanostructures, Semiconductors 38 (2004) 99–106.

[16] P. Landsberg, Trap-Auger recombination in silicon of low carrier densities, Appl. Phys. Lett. 50 (1987) 745–747, https://doi.org/10.1063/1.98086.

[17] J. Murphy, K. Bothe, R. Krain, V. Voronkov, R. Falster, Parameterisation of injection-dependent lifetime measurements in semiconductors in terms of Shockley-Read-Hall statistics: an application to oxide precipitates in silicon, J. Appl. Phys. 111 (2012) 113709, https://doi.org/10.1063/1.4725475.

[18] C. Sun, F.E. Rougieux, D. Macdonald, A unified approach to modelling the charge state of monatomic hydrogen and other defects in crystalline silicon, J. Appl. Phys. 117 (2015) 045702, https://doi.org/10.1063/1.4906465.

[19] Henry, Lang, Nonradiative capture and recombination by multiphonon emission in GaAs and GaP, Phys. Rev. B 15 (1977) (989–101).

[20] M. Lax, Cascade capture of electrons in solids, Phys. Rev. 119 (1960) 1502–1523.

[21] L.C. Kimerling, Recombination enhanced defect reactions, Solid-State Electron. 21 (1978) 1391–1401, https://doi.org/10.1016/0038-1101(78)90215-0.

[22] P.T. Landsberg, D.J. Robbins, The first 70 semiconductor Auger processes, Solid-State Electron. 21 (1978) 1289–1294, https://doi.org/10.1016/0038-1101(78)90195-8.

[23] V.N. Abakumov, V.I. Perel, I.N. Yassievich, Modern problems in condensed matter sciences, ScienceDirect 33 (1991), https://doi.org/10.1016/B978-0-444-88854-9.50006-0 (xi).

[24] D.A. Evans, P.T. Landsberg, Recombination statistics for auger effects with applications to p-n junctions, Solid-State Electron. (1963), https://doi.org/10.1016/0038-1101(63)90012-1.

[25] Hangleiter, Nonradiative recombination via deep impurity levels in silicon: experiment, Phys. Rev. B Condens. Matter 35 (1987) 9149–9161, https://doi.org/10.1103/PhysRevB.35.9149.

[26] M. Combescot, Thermodynamics of an electron—hole system in semiconductors, Phys. Status Solidi (B) 86 (1978) 349–358, https://doi.org/10.1002/pssb.2220860141.

[27] D. Kane, Ranson, The effect of excitons on apparent band gap narrowing and transport in semiconductors, J. Appl. Phys. 73 (1993) 1193–1197, https://doi.org/10.1063/1.353285.

[28] W. Bludau, A. Onton, W. Heinke, Temperature dependence of the band gap of silicon, J. Appl. Phys. 45 (1974) 1846–1848, https://doi.org/10.1063/1.1663501.

[29] M.A. Green, Intrinsic concentration, effective densities of states, and effective mass in silicon, J. Appl. Phys. 67 (1990) 2944–2954, https://doi.org/10.1063/1.345414.

[30] J. Frenkel, On pre-breakdown phenomena in insulators and electronic semi-conductors, Phys. Rev. 54 (1938) 647–648, https://doi.org/10.1103/PhysRev.54.647.

[31] J.M. Herman, C.T. Sah, Thermal capture of electrons and holes at zinc centers in silicon, Solid-State Electron. 16 (1973) 1133–1139, https://doi.org/10.1016/0038-1101(73)90140-8.

[32] A. Schenk, A model for the field and temperature dependence of Shockley-Read-Hall lifetimes in silicon, Solid-State Electron. 35 (1992) 1585–1596, https://doi.org/10.1016/0038-1101(92)90184-E.

[33] H. Pettersson, H.G. Grimmeiss, T. L, Electrical and optical properties of molybdenum and tungsten related defects in silicon, Semicond. Sci. Technol. 6 (1991) 237–242.

[34] K.R. McIntosh, B.B. Paudyal, D.H. Macdonald, Generalized procedure to determine the dependence of steady-state photoconductance lifetime on the occupation of multiple defects, J. Appl. Phys. 104 (2008) 084503, https://doi.org/10.1063/1.2999640.

[35] P. Blood, O.J. on in Physics, The electrical characterisation of semiconductors, 1978.

[36] D. Lang, Deep-level transient spectroscopy: a new method to characterize traps in semiconductors, J. Appl. Phys. 45 (1974) 3023–3032, https://doi.org/10.1063/1.1663719.

[37] L. Dobaczewski, A.R. Peaker, K. Bonde Nielsen, Laplace-transform deep-level spectroscopy: The technique and its applications to the study of point defects in semiconductors, J. Appl. Phys. (2004).

[38] W. Kwapil, J. Schon, W. Warta, M.C. Schubert, Carrier recombination at metallic precipitates in p-and n-type silicon, IEEE J. Photovolt. 5 (2015) 1285–1292, https://doi.org/10.1109/JPHOTOV.2015.2438634.

[39] Kwapil, Schon, Warta, Schubert, Erratum to carrier recombination at metallic precipitates in p- and n-type silicon [Sep 15 1285–1292], IEEE J. Photovolt. 6 (2016) (391–391).

[40] J. Kaniewski, M. Kaniewska, A. Peaker, Deep levels associated with oxidation induced stacking faults in n-type silicon, Appl. Phys. Lett. 60 (1992) 359–361, https://doi.org/10.1063/1.106656.

[41] K. Knobloch, M. Kittler, W. Seifert, Influence of contamination on the dislocation-related deep level C1 line observed in deep-level-transient spectroscopy of n-type silicon: a comparison with the technique of electron-beam-induced current, J. Appl. Phys. 93 (2003) 1069–1074, https://doi.org/10.1063/1.1532938.

[42] P. Omling, E.R. Weber, L. Montelius, H. Alexander, J. Michel, Electrical properties of dislocations and point defects in plastically deformed silicon, Phys. Rev. B 32 (1985) 6571–6581.

[43] T. Kieliba, S. Riepe, W. Warta, Effect of dislocations on minority carrier diffusion length in practical silicon solar cells, J. Appl. Phys. 100 (2006) 063706.

[44] C. Donolato, M. Bianconi, Use of the EBIC contrast profile area for evaluating the recombination strength of dislocations, Phys. Status Solidi (a) 102 (1987) K7–K11.

[45] V. Kveder, M. Kittler, W. Schröter, Recombination activity of contaminated dislocations in silicon: a model describing electron-beam-induced current contrast behavior, Phys. Rev. B 63 (2001) 115208.

[46] R. Gibb, G. Rees, B. Thomas, B. Philosophical, A two stage model for deep level capture, 1977. ⟨http://dx.doi.org/10.1080/14786437708239776⟩.

[47] A.C. Wang, C. Sah, Complete electrical characterization of recombination properties of titanium in silicon, J. Appl. Phys. 56 (1984) 1021–1031, https://doi.org/10.1063/1.334095.

[48] T. Sadoh, H. Nakashima, T. Tsurushima, Deep levels of vanadium and vanadium-hydrogen complex in silicon, J. Appl. Phys. 72 (1992) 520–524.

[49] Conzelmann, Graff, Weber, Chromium and chromium-boron pairs in silicon, Appl. Phys. A Solids Surf. 30 (1983) 169–175.

[50] C. Sun, F.E. Rougieux, D. Macdonald, Reassessment of the recombination parameters of chromium in n- and p-type crystalline silicon and chromium-boron pairs in p-type crystalline silicon, J. Appl. Phys. 115 (2014) 214907.

[51] A.A. Istratov, H. Hieslmair, E.R. Weber, Iron and its complexes in silicon, Appl. Phys. A: Mater. Sci. Process. 69 (1999) 13–44.

[52] B. Paudyal, K. Mcintosh, D. Macdonald, Tempreature dependent electron and hole capture cross sections of iron-contaminated boron-doped silicon, in: Proceedings of the 34th IEEE Photovoltaic Specialists Conference (PVSC), 2009, pp. 001588–001593. ⟨http://dx.doi.org/10.1109/PVSC.2009.5411380⟩.

[53] C.-T. Sah, P. Chan, C.-K. Wang, R.-Y. Sah, K.A. Yamakawa, Lutwack, Effect of zinc impurity on silicon solar-cell efficiency, IEEE Trans. Electron Devices 28 (1981) 304–313.

[54] J. Benton, D. Jacobson, B. Jackson, J. Johnson, T. Boone, D. Eaglesham, F. Stevie, J. Becerro, Behavior of molybdenum in silicon evaluated for integrated circuit processing, J. Electrochem. Soc. 146 (1999) 1929–1933, https://doi.org/10.1149/1.1391868.

[55] B.B. Paudyal, K.R. McIntosh, D.H. Macdonald, G. Coletti, Temperature dependent

carrier lifetime studies of Mo in crystalline silicon, J. Appl. Phys. 107 (2010) 054511, https://doi.org/10.1063/1.3309833.
[56] S. Diez, S. Rein, S.W. Glunz, Analyzing defect by temperature and injection dependent lifetime spectroscopy (T-IDLS), in: Proceedings of the 20th European Photovoltaic Solar Energy Conference, 6-10 June 2005, Barcelona, Spain. (n.d.).
[57] R.H. Wu, A.R. Peaker, Capture cross sections of the gold donor and acceptor states in n-type Czochralski silicon, Solid-State Electron. 25 (1982) 643–649, https://doi.org/10.1016/0038-1101(82)90066-1.
[58] J.M. Hwang, D.K. Schroder, Recombination properties of oxygen-precipitated silicon, J. Appl. Phys. 59 (1986) 2476–2487.
[59] B. Hallam, M. Kim, M. Abbott, N. Nampalli, T. Nærland, B. Stefani, S. Wenham, Recent insights into boron-oxygen related degradation: evidence of a single defect, Sol. Energy Mater. Sol. Cells 173 (2017) 25–32, https://doi.org/10.1016/j.solmat.2017.06.038.
[60] T. Niewelt, J. Schön, J. Broisch, W. Warta, M. Schubert, Electrical characterization of the slow boron oxygen defect component in Czochralski silicon, Phys. Status Solidi RRL 9 (2015) 692–696.
[61] T. Niewelt, S. Mägdefessel, M.C. Schubert, Fast in-situ photoluminescence analysis for a recombination parameterization of the fast BO defect component in silicon, J. Appl. Phys. (2016).
[62] V.V. Voronkov, R. Falster, K. Bothe, Lifetime-degrading boron-oxygen centres in p-type and n-type compensated silicon, J. Appl. Phys. 110 (2011) 063515.
[63] P. Wagner, J. Hage, Thermal double donors in silicon, Appl. Phys. A Solids Surf. 49 (1989) 123–138, https://doi.org/10.1007/BF00616290.
[64] M. Tomassini, J. Veirman, R. Varache, E. Letty, S. Dubois, Y. Hu, Ø. Nielsen, Recombination activity associated with thermal donor generation in monocrystalline silicon and effect on the conversion efficiency of heterojunction solar cells, J. Appl. Phys. 119 (2016) 084508, https://doi.org/10.1063/1.4942212.
[65] T. Mchedlidze, J. Weber, Direct detection of carrier traps in Si solar cells after light-induced degradation, Phys. Status Solidi (RRL) - Rapid Res. Lett. 9 (2015) 108–110, https://doi.org/10.1002/pssr.201409474.
[66] K. Bothe, R. Sinton, J. Schmidt, Fundamental boron–oxygen-related carrier lifetime limit in mono- and multicrystalline silicon, Progress. Photovolt.: Res. Appl. 13 (2005) 287–296, https://doi.org/10.1002/pip.586.